Journal of Materials Chemistry B

PAPER

View Article Online
View Journal | View Issue

Cite this: J. Mater. Chem. B, 2019, 7, 7363

Bypassing pro-survival and resistance mechanisms of autophagy in EGFR-positive lung cancer cells by targeted delivery of 5FU using theranostic Ag_2S quantum dots

Fatma Demir Duman,†[a] Yunus Akkoc,†[b] Gozde Demirci,[c] Nima Bavili,[d] Alper Kiraz,[cd] Devrim Gozuacik *[be] and Havva Yagci Acar *[acf]

Received 31st July 2019,
Accepted 10th October 2019

DOI: 10.1039/c9tb01602c

rsc.li/materials-b

Targeted drug delivery systems that combine imaging and therapeutic functions in a single structure have become very popular in nanomedicine. Near-infrared (NIR) emitting Ag_2S quantum dots (QDs) are excellent candidates for this task. Here, we have developed PEGylated Ag_2S QDs functionalized with Cetuximab (Cet) antibody and loaded with an anticancer drug, 5-fluorouracil (5FU). These theranostic QDs were used for targeted NIR imaging and treatment of lung cancer using low (H1299) and high (A549) Epidermal Growth Factor Receptor (EGFR) overexpressing cell lines. The Cet conjugated QDs effectively and selectively delivered 5FU to A549 cells and provided significantly enhanced cell death associated with apoptosis. Interestingly, while treatment of cells with free 5FU activated autophagy, a cellular mechanism conferring resistance to cell death, these EGFR targeting multimodal QDs significantly overcame drug resistance compared to 5FU treatment alone. The improved therapeutic outcome of 5FU delivered to A549 cells by Cet conjugated Ag_2S QDs is suggested as the synergistic outcome of enhanced receptor mediated uptake of nanoparticles, and hence the drug, coupled with suppressed autophagy even in the absence of addition of an autophagy suppressor.

Introduction

Cancer is one of the most challenging diseases to cure, and the leading cause of death around the world.[1,2] Surgical resection of the tumour, and conventional chemo- and radiotherapy are the most adopted treatment approaches in the clinic.[3] However, each of these strategies has its own limitations. The most frequent challenges encountered in today's cancer therapy include tumour metastasis, residual disease burden, non-specific systemic distribution of chemotherapeutic agents, insufficient drug concentration reaching the tumorous tissues and occurrence of multiple drug resistance in cancer cells. On the other hand, early detection and diagnosis of cancer is very critical to succeed in cancer therapy and improve patients' survival rates. The predominant techniques for the current clinical detection and diagnosis of cancer include magnetic resonance imaging, ultrasound, computerized tomography, positron emission tomography and X-rays. However, there is still a need for sensitive and safe techniques with high specificity to detect cancer, particularly in the early stage.[4,5]

Development of semiconductor quantum dots (QDs) with strong and stable luminescence has created a new possibility for optical imaging. Use of QDs in cancer detection has emerged as a non-invasive, high-resolution and real-time optical method with many advantages over conventional modalities.[6] NIR emitting QDs have greater importance for medical use compared to most frequently used commercial QDs emitting in the visible region of the optical spectrum (400–700 nm).[7,8] The low photon penetration depth of visible light, absorption and scattering of light by hemoglobin and deoxyhemoglobin, and significant auto-fluorescence of collagen in living tissues make the visible window impractical for optical contrast generation.[9] However, imaging in the NIR-I region (700–900 nm) enhances the sensitivity and resolution by eliminating the scattering and absorption effects as well as the auto-fluorescence and, hence, increases the

[a] Koc University, Department of Chemistry, 34450 Istanbul, Turkey. E-mail: fyagci@ku.edu.tr; Tel: +90 (212) 338 1742
[b] Sabanci University, Faculty of Engineering and Natural Sciences, Molecular Biology, Genetics and Bioengineering Programs, 34956 Istanbul, Turkey. E-mail: dgozuacik@sabanciuniv.edu; Tel: +90-216-483 9617
[c] Koc University, Graduate School of Materials Science and Engineering, Rumelifeneri Yolu, Sariyer, 34450 Istanbul, Turkey
[d] Koc University, Department of Physics, Rumelifeneri Yolu, Sariyer, 34450 Istanbul, Turkey
[e] Sabanci University, Center of Excellence for Functional Surfaces and Interfaces for NanoDiagnostics (EFSUN), 34956 Istanbul, Turkey
[f] KUYTAM, Koc University Surface Science and Technology Center, 34450 Istanbul, Turkey
† These authors contributed equally to this work.

signal/noise ratio. In addition, light penetrates deeper into tissues at such longer wavelegths allowing deeper tissue imaging. For these reasons, the NIR region between 700 and 900 nm is known as the therapeutic window or the optical window for biomedical applications.[10] Ag_2S QDs are among the most promising NIR-emitting QDs with high biocompatibility compared to traditional Cd- or Pb-based QDs such as CdTe(II–VI),[11] PbS(IV–VI),[12] or core/shell quantum dots (CdTe/CdSe, CdSe/CdTe and CdSe/ZnTe).[13–15] The first photoluminescent Ag_2S QDs were reported by Wang *et al.* in 2010.[16] They synthesized hydrophobic Ag_2S NIR QDs emitting at 1058 nm using $(C_2H_5)_2NCS_2Ag$ and transferred them into water *via* ligand exchange with DHLA and PEGylation.[17] These Ag_2S NIRQDs showed enhanced spatial resolution in the *in vivo* imaging of angiogenesis[17] and allowed tracking of mesenchymal stem cells *in vivo*.[18] Combination of Ag_2S QDs with Gd provided dual-mode imaging in brain surgery, taking advantage of the high spatiotemporal resolution of fluorescence imaging in the second near-infrared window (NIR-II) and deep tissue penetration of enhanced magnetic resonance imaging.[19] Due to their ultralow solubility product constants ($K_{sp}(Ag_2S) = 6.3 \times 10^{-50}$; $K_{sp}(CdS) = 8.0 \times 10^{-27}$; $K_{sp}(CdSe) = 6.31 \times 10^{-36}$), the release of Ag ions into biological systems is very low and this makes Ag_2S QDs excellent probes for optical bioimaging.[20–22] Reports on the long-term *in vivo* effects of Ag_2S QDs indicate no appreciable cytotoxicity at the tested doses (15 and 30 mg kg^{-1}) over a period of 2 months and claim a highly biocompatible nature as well as NIR imaging potential *in vivo*.[23]

The high surface to volume ratio of QDs and functional coating materials allow loading of therapeutic agents such as drugs, oligonucleotides and peptides as well as decoration with targeting ligands for site-specific delivery.[24–30] Hence, QDs have created great promise as new generation theranostics. Ag_2S QDs are efficiently employed as therapeutic agents besides their diagnostic/imaging properties. Chen *et al.* demonstrated targeted cancer therapy using cyclic RGD peptide (cRGD)-tagged Ag_2S QDs loaded with doxorubicin based on the 2MPA coated Ag_2S that we have previously reported.[31] Wang *et al.* reported bovine serum albumin (BSA)-stabilized NIR-emitting Ag_2S QDs and their conjugation with endothelial growth factor (VEGF) antibody for targeted cancer imaging.[28] We have designed and used folate-targeted doxorubicin-loaded Ag_2S QDs for drug delivery into folate-receptor overexpressing cancer cells.[32,33] Selective delivery of QDs and their cargo to the tumour site is crucial to reduce the effective therapeutic dose range and improve the drug efficacy while reducing off-site effects.[34] In other words, molecularly targeted therapies have the potential to improve patient outcomes over traditional chemotherapies and reduce the side effects.[35,36]

Epidermal growth factor receptor (EGFR) is a cell surface receptor that is either amplified or mutated in the majority of cancers including lung, colorectal, breast *etc.* and originates from the epithelium.[37,38] EGFR is also one of the widely studied signal transducers with an active role in regulation of several key phenomena of cancer including proliferation, tumour metastases, and angiogenesis.[39] Thus, targeting of EGFR with a ligand which has high affinity for the receptor has been conceived as an attractive cancer treatment strategy in the last decades.[40–42] Cetuximab (Erbitux®, C225, Cet) is an immunoglobulin G1 mouse–human chimeric monoclonal antibody that binds specifically to the external domain of EGFR with high affinity. It inhibits signal transduction and blocks EGFR signalling cascades.[43] Therefore, Cet exhibits effective targeting and therapy in clinical applications, especially when combined with chemotherapy.[44,45]

5-Fluorouracil (5FU), a pyrimidine analogue with antimetabolite activity, is a chemotherapy drug widely employed in cancer treatment. The drug inhibits synthesis of DNA, acting as a competitive inhibitor of three enzymes in the pyrimidine metabolism.[46] However, 5FU presents a short half-life (10–20 min), low tumour affinity, wide distribution and various side effects in patients. In addition, drug resistance and tumour heterogeneity decrease the effectiveness of the drug.[47] Of note, autophagy was identified as a key mechanism in the cellular response to 5FU.[48,49] In many studies, 5FU treatment resulted in an increase in autophagy, and subsequent protection of cancer cells against drug-induced apoptosis.[48,50–53] Therefore, inhibition of the cyto-protective autophagy may be an effective strategy to enhance apoptosis and facilitate the activity of anti-cancer agents. Pan *et al.* showed that pre-treatment of A549 cells (adenocarcinomic human alveolar basal epithelial cell line) with 3-methyladenine (3-MA), an inhibitor of autophagy, and knock down of AATG7 expression using ATG7 siRNA inhibit autophagy and hence promote 5FU-induced apoptosis by inducing ROS formation.[54] Liang *et al.* also reported enhanced 5FU mediated death in human gall bladder carcinoma cell lines after suppression of autophagy by chloroquine (CQ) pre-treatment.[55] Such an approach may provide a great therapeutic outcome especially if it is coupled with selective delivery of these agents to the tumour site in effective concentrations, which may be achieved by nanoparticulate delivery vehicles.

In this study, we developed theranostic Ag_2S QDs, which can be fluorescently detected in the NIR-optical imaging window, targeting 5FU to EGFR positive lung cancer cell lines. We have previously reported the synthesis, imaging and gene delivery potential of the first cationic Ag_2S QDs with exceptionally high quantum yield and stability.[56] Here, we decorated their surfaces with poly(ethylene glycol) (PEG) to enhance their biocompatibility and blood circulation half-life, tagged them with Cet to target and detect EGFR overexpressing cancer cells with high imaging efficiency, and loaded with 5FU for targeted delivery of the drug to the selected cell line. EGFR overexpressing A549 (adenocarcinomic human alveolar basal epithelial cell line) cells and EGFR low-expressing H1299 (human non-small cell lung carcinoma) cells were used to confirm the targeted delivery of the QDs after Cet antibody conjugation. To assess the theranostic potential of the QDs, *in vitro* optical imaging, cytotoxicity, uptake and apoptosis studies were conducted in detail. Moreover, we discovered that the 5FU loaded Cet conjugated-Ag_2S QDs overcome 5FU-induced cyto-protective autophagy and enhance cell death in an EGFR status dependent manner without application of any autophagy inhibitors.

Materials and methods

Materials

Silver nitrate ($AgNO_3$, 99.9999%) and 2-(*N*-morpholino)ethanesulfonic acid (MES) were purchased from Sigma-Aldrich (St. Louis, MO, USA). Branched PEI (25 kDa molecular weight (MW)) and *N*,*N*′-carbonyldiimidazole (CDI) were purchased from Aldrich (Darmstadt, Germany). Sodium sulfide (Na_2S) and 1-ethyl-3-(3-dimethylaminopropyl)carbodiimide (EDC) were provided by Alfa-Aesar (Lancashire, UK). Methoxy(polyethylene glycol) (mPEG–OH, 2 kDa) was purchased from Rapp Polymere, (Tubingen, Germany). Amine–polyethylene glycol–valeric acid (amine–PEG–VA, 3.4 kDa) was obtained from Laysan Bio Inc. (Arab, AL, USA). *N*-Hydroxysuccinimide (NHS), sodium hydroxide, ethanol, acetic acid, chloroform, tetrahydrofuran and suprapur nitric acid (65%) were purchased from Merck Millipore (Bedford, MA, USA). Cetuximab (Cet) was obtained from Merck (Erbitux®; Merck KgaA, Darmstadt, Germany). 5-Fluorouracil (5FU; > 99.0%) was provided by Tokyo Chemical Industry (TCI, Tokyo, Japan). The Coomassie Plus (Bradford) Assay Kit (Pierce; #23236) was purchased from Thermo Scientific (Rockford, IL, USA). A dialysis membrane (Cellu·Sep T1, MWCO 3.5 Da) was purchased from Membrane Filtration Products, Inc. (Seguin, TX, USA). Vivaspin 20 centrifugal filters (10, 30 and 100 kDa MW cut-off) were purchased from Sartorius (Goettingen, Germany). Roswell Park Memorial Institute (RPMI) 1640 medium (with L-glutamine and 25 mM HEPES), and penicillin–streptomycin and trypsin–EDTA solutions were purchased from Multicell, Wisent Inc. (St. Bruno, QC, Canada). Fetal bovine serum (FBS) was purchased from Capricorn Scientific GmbH (Ebsdorfergrund, Germany). Phosphate buffered saline (PBS) tablets and thiazolyl blue tetrazolium bromide (MTT) were obtained from Biomatik Corp. (Cambridge, ON, Canada). Dimethyl sulfoxide Hybri-Max™ and 4′,6-diamidino-2-phenylindole (DAPI) were provided by Sigma (St. Louis, MO, USA) and 4% paraformaldehyde solution (in PBS) was provided by Santa Cruz Biotechnology, Inc. (Santa Cruz, CA, USA). All 12, 24 and 96-well plates were purchased from Nest Biotechnology Co. Ltd (Wuxi, China).

Only Milli-Q water (18.2 MOhm) (Rephile Biosciences and Technology, Shanghai, China) was used when necessary. All reagents were of analytical grade or of the highest purity.

A549 (adenocarcinomic human alveolar basal epithelial cell line) and H1299 (human non-small cell lung carcinoma) cells were given as a gift from Dr Ferda Ari (Uludag University, Department of Biology, Bursa, Turkey).

Preparation of Ag_2S QDs

Ag_2S QDs were prepared according to our previous report using branched PEI (25 kDa) and 2MPA as a coating.[56] Briefly, 1.25 mmol of $AgNO_3$ was dissolved in 375 mL of deoxygenated water under vigorous mechanical stirring (5000 rpm) at room temperature (RT: 25 °C). PEI (14.25×10^{-3} mmol) and 2MPA (1.25 mmol) were added into this solution under an argon atmosphere. The pH of the solution was set to 9 using NaOH (1 M) and acetic acid (1 M). In parallel, 0.3125 mmol of Na_2S was dissolved in 125 mL of deoxygenated water in a round bottom flask and transferred into the reaction mixture. After stirring for 5 min, the resulting brown solution was washed through Vivaspin 20 centrifugal filters (30 kDa MW) to remove unreacted chemicals. The product was lyophilized for further applications. All samples were kept in the dark. The samples in the powder form were stored at −20 °C, whereas the liquids were stored at 4 °C.

Preparation of CDI-activated methoxy-PEG (mPEG–CDI)

Methoxy(polyethylene glycol) (mPEG–OH, 2 kDa) was activated by *N*′-carbonyldiimidazole (CDI) in order to conjugate the hydroxyl terminal groups to amine groups of branched PEI on the Ag_2S QDs using a similar approach to that of Chen *et al.*[57] According to the procedure, mPEG–OH (4.0 g) was dissolved in anhydrous THF (30 mL) after vacuum-drying at 60 °C for 8 h. CDI (3.2 g) was dissolved in THF (20 mL) and mPEG–OH solution was added dropwise to this solution. The mixture was stirred under an argon atmosphere for 24 h and finally the reaction was terminated with 200 μL of distilled water. The reaction solution was added into a large excess of cold diethyl ether under vigorous agitation. The precipitate was collected by centrifugation and dried under a vacuum.

mPEG–CDI conjugation of Ag_2S QDs (mPEG–Ag_2S QDs)

PEI/2MPA coated Ag_2S QDs were PEGylated as shown in Scheme 1 to obtain mPEG conjugated Ag_2S QDs (mPEG–Ag_2S QDs). Briefly, Ag_2S QDs (300 mg) and CDI activated mPEG (2182 mg) were dissolved in 50 mL of anhydrous chloroform and the mixture was stirred at RT for 24 h. The resulting product was dried using a rotary evaporator at 40 °C (Laborota 4000, Heidolph, Germany) and a Nuve EV 018 vacuum oven (Ankara, Turkey) at RT, consecutively. Then, the dried sample was washed with deionized water using Vivaspin 20 centrifugal filters (30 kDa MW) and stored at −20 °C after being lyophilized.

Cetuximab conjugation of mPEG–Ag_2S QDs (mPEG–Ag_2S–Cet)

Amine–polyethyleneglycol–valeric acid (NH_2–PEG–VA, MW 3.4 kDa) was used as a linker to conjugate mPEG–Ag_2S QDs with cetuximab (Cet). First, 0.066 μmol (0.224 mg) amine–PEG–VA was dissolved in 2 mL of MES buffer (0.1 M, pH 6.0) and activated with 0.0132 mmol of EDC (2.53 mg) and 0.0132 mmol NHS (1.52 mg) for 2 min. Then, 827.5 mg of mPEG–Ag_2S QDs were added to this mixture and stirred at RT for 24 h. The reaction mixture was washed with PBS (pH 7.4, 1×) using Vivaspin 20 centrifugal filters with a 30 kDa MW cut-off.

As a second step, 20 mL of cetuximab solution (5 mg mL^{-1}) was washed with PBS buffer (pH 7.4, 1×) using 10 kDa MW cut-off centrifugal filters and its concentration was determined using a Bradford protein assay kit according to the manufacturer's instructions (Coomassie Plus Protein Assay Reagent, Pierce). 2.778 mL of cetuximab solution (3.6 mg mL^{-1}, 0.066 μmol), 0.0132 mmol EDC (2.53 mg) and 0.0132 mmol NHS (1.52 mg) were added into 12.5 mL of MES buffer (0.1 M, pH 6.0) and stirred at RT for 2 min. Finally, the VA–PEG–NH_2 linked mPEG–Ag_2S QD solution was introduced into this mixture and stirred at RT for 24 h. The resulting conjugates were washed with PBS through centrifugal filters (100 kDa MW cut-off) and the cetuximab

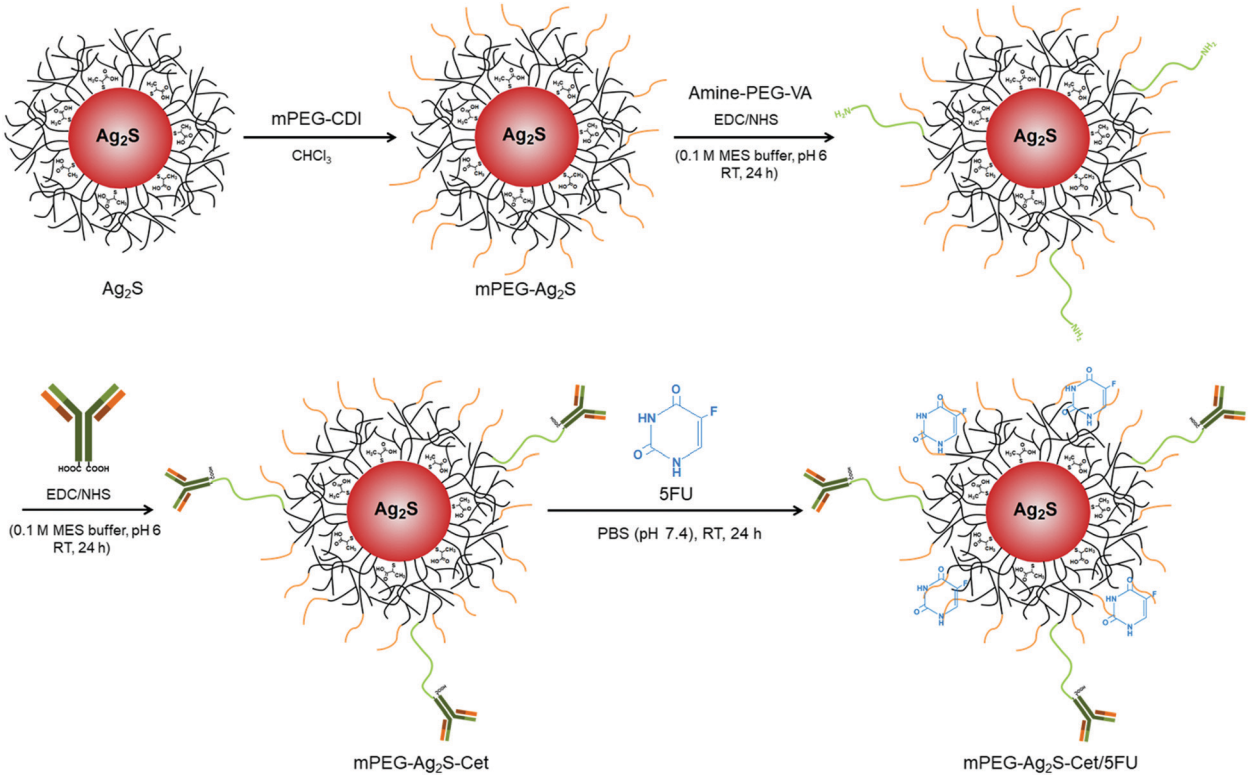

Scheme 1 Synthesis of Ag_2S, mPEG–Ag_2S, mPEG–Ag_2S–Cet and mPEG–Ag_2S–Cet/5FU QDs.

conjugation efficiency was measured using a Bradford protein assay kit (n = 3).

5FU loading of mPEG–Ag_2S–Cet QDs (mPEG–Ag_2S–Cet/5FU)

For 5-fluorouracil (5FU) loading, 341.25 mg of mPEG–Ag_2S–Cet QDs and 40 mg of 5FU were dissolved in PBS (pH 7.4, 1×) and stirred for 20 h at RT. Then, the complexes were dialyzed against PBS using a cellulose dialysis membrane (MW cut-off 3500 Da) for 3 h changing the PBS once every 1.5 h to remove unloaded 5FU. The amount of the loaded drug was calculated from the unloaded 5FU in the dialysis solution using a standard absorbance calibration curve of 5FU at 265 nm and subtracted from the initial loading to find the weight of the loaded drug. The drug encapsulation efficiency (EE%) expressed as the percentage of the drug amount in the nanoparticles over the total amount used initially and the drug loading efficiency (LE%) expressed as the percentage of the drug amount found in the nanoparticles were calculated using the following equations:

$$\text{5FU EE\%} = \frac{\text{Weight of loaded drug}}{\text{Weight of initial loading}} \times 100\% \quad (1)$$

$$\text{5FU LE\%} = \frac{\text{Weight of loaded drug}}{\text{Weight of drug loaded QDs}} \times 100\% \quad (2)$$

Characterization methods

Absorbance spectra were recorded on a Shimadzu 3101 PC UV-vis-NIR spectrophotometer in the 200–550 nm region. Photoluminescence spectra in the NIR region (600–1100 nm spectral range) were recorded by using a homemade setup equipped with a 1/8 Newport Cornerstone 130 monochromator with 600 L per mm grating. The frequency doubled output of a DPSS laser working at 532 nm was used for the excitation and a 590 nm long pass filter was used for the emission. A Si detector (Thorlabs PDF10A, 1.4 × 10^{-15} W $Hz^{-1/2}$) was used in the setup. The slit width was fixed at 0.5 mm during the measurements. The quantum yield (QY) of the Ag_2S QDs was calculated with respect to LDS 798 NIR dye from Exciton, which has a 14% QY in MeOH, as described in ref. 56.

The hydrodynamic size and zeta potential of QDs in water were determined using a Malvern Zetasizer Nano-ZS. All measurements were carried out in triplicate. The Ag content in the QD solutions was determined using an Agilent 7700× Inductively Coupled Plasma Mass Spectrometer (ICP-MS) according to a standard calibration curve of Ag (n = 3). An acid digestion procedure with suprapur nitric acid 65% (0.5 mL) was applied to the QD solutions and the acidified samples were diluted with deionized water to a total volume of 10 mL before the measurements. All measurements except ICP-MS were performed in PBS solution. ICP-MS measurements were managed in water to prevent the interference of Ag by other ions in the solutions.

ICP analysis and nanoparticle concentration calculations were performed with samples filtered through 0.2 μm sterile nylon syringe filters considering the possible concentration change during the sterile filtration performed for *in vitro* studies.

Cell culture

EGFR-overexpressing A549 (adenocarcinomic human alveolar basal epithelial cell line) and EGFR low-expressing H1299

(human non-small cell lung carcinoma) cells were cultured in RPMI 1640 cell culture medium supplemented with 10% FBS and 100 U/100 mg per mL penicillin/streptomycin and grown in a humidified incubator at 37 °C under 5% CO_2. The cells reaching confluence were washed with PBS and detached with trypsin–EDTA.

In vitro cytotoxicity studies

In vitro cytotoxicity studies were performed using 3-(4,5-dimethylthiazol-2-yl)-2,5-diphenyl tetrazolium bromide (MTT, M5665, Sigma, St. Louis, MO) colorimetric assay. A549 and H1299 cells were seeded at a density of 1×10^4 cells per well into 96-well plates and incubated at 37 °C under 5% CO_2. On the second day, the cells were treated with different concentrations of Ag_2S, mPEG–Ag_2S, mPEG–Ag_2S–Cet, and mPEG–Ag_2S–Cet/5FU based on their Ag content to achieve a fixed particle number between different formulations, or with free Cet and free 5FU in equivalent concentrations to the Cet and 5FU content of the QDs for comparison. After 48 h incubation, the medium in each well was replenished with 50 μL of MTT solution (5 mg mL^{-1} in PBS) and 150 μL of fresh culture medium, and incubation was extended for 4 more hours at 37 °C in 5% CO_2. The purple formazan crystals formed during incubation with MTT were dissolved with DMSO/EtOH (1 : 1 v/v) solution. The absorbance at 600 nm was read by a microplate reader (BioTek ELx800 Absorbance Microplate Reader) with a reference reading at 630 nm. The absorbance intensity of the QD-treated cells without MTT treatment was determined to eliminate the QD-dependent absorbance in the MTT readings. Cells without QD, 5FU or Cet treatment were considered as a control. The relative cell viability was calculated using the equation shown below (n = 4):

$$\text{Cell viability } (\%) = \left[\frac{\text{sample absorbance}}{\text{control absorbance}}\right] \times 100 \qquad (3)$$

Intracellular uptake and NIR fluorescence imaging of QDs

The intracellular NIR emission intensities and the differences in cellular internalization and localization of Ag_2S, mPEG–Ag_2S, mPEG–Ag_2S–Cet and mPEG–Ag_2S–Cet/5FU QDs were investigated in EGFR-overexpressing A549 cells and EGFR low-expressing H1299 cells by fluorescence microscopy. The two cell lines were seeded at a density of 175 000 cells into glass bottom dishes and incubated for 24 h at 37 °C in 5% CO_2. Each sample was introduced to the cells at a concentration of 5 μg Ag per mL. Untreated cells were used as controls. After incubation for an additional 24 h at 37 °C in 5% CO_2, the cells were left in 4% paraformaldehyde solution at RT for 20 min for fixation and stained with DAPI nuclear dye (2 μg mL^{-1}) by washing with PBS three times at each step. 2 mL PBS was left in each well to protect the cells against air-drying. The experimental set-up used for fluorescence imaging included a frequency doubled femtosecond-pulsed Ti:Sa solid-state tunable laser source (Chameleon Ultra II, Coherent). The laser was tuned to 488 nm and 400 nm for the QD and DAPI measurements, respectively. The laser beam was directed through several mirrors and a Keplerian telescope to an inverted microscope (Nikon, Eclipse TE2000-U) equipped with a dichroic mirror (Q495LP, Chroma) and a 60× oil-immersion objective (Nikon Apo TIRF, NA = 1.49). A 300 mm focal length lens was used to focus the laser at the back focal plane of the microscope objective in order to obtain wide field illumination. Fluorescence images were captured by an EMCCD camera (ImagEM, Hamamatsu) with 5 and 20 second exposure times for QD and DAPI measurements, respectively. A long pass filter (RG665 and FGL435 for QD and DAPI imaging, respectively) was placed in front of the camera for rejecting the excitation laser light. The recorded images were processed by ImageJ software (version 1.46r, NIH, USA).[58]

Cell death analysis by FACS

Apoptosis and necrosis were determined by fluorescence-activated cell sorting (FACS) analyses. In the cell death assay, after treatment of the cells with the QD formulations at 5 μg mL^{-1} Ag concentration and the equivalent free Cet and free 5FU for 48 h, floating and adherent cells were first collected, washed twice with ice-cold 1× PBS and centrifuged at 1200 rpm for 5 min. The pellet was dissolved in 1× Annexin-V binding buffer (10 mM HEPES (pH 7.4), 150 mM NaCl, 2.5 mM $CaCl_2$ in PBS (pH 7.4)). Then, RNase (100 μg mL^{-1}), PI (40 μg mL^{-1}, P3566, Invitrogen, Eugene, OR) and FITC-Annexin V (1 mg mL^{-1}) were added to the solution. The samples were then incubated for 10 min in the dark on ice. FACscan analyses of PI and FITC positivity were performed using a BD FACS Canto flow cytometry system (BD, San Jose, CA) and analysed using the FlowJo Program. At least 10 000 events were analyzed per experimental point.

Immunoblot analysis and antibodies

Protein extraction was performed with RIPA buffer (50 mM Tris–HCl pH 7.4, 150 mM NaCl, 1% NP40, 0.25% Na-deoxycholate) supplemented with complete protease inhibitor cocktail (Roche, 04-693-131-001) and 1 mM phenylmethylsulfonyl fluoride (PMSF; Sigma-Aldrich, P7626). The cell extracts treated with the QD formulations at 5 μg mL^{-1} Ag concentration and the equivalent free 5FU for 48 h (30 μg for p62 degradation and LC3 shift analysis; 100 μg for the apoptosis related protein analysis) were separated by SDS-polyacrylamide gels and transferred to a nitrocellulose membrane. Following blockage in 5% nonfat milk, the membranes were incubated in 3% BSA–PBST solutions containing primary antibodies (ab): anti-LC3B ab (CST, #2775, 1 : 1000), anti-SQSTM1/p62 ab (BD Transduct. Lab, 610832, 1 : 4000), anti-Caspase-3 ab (CST, #9662, 1 : 1000), anti-Cleaved-Caspase-3 ab (CST, #9664, 1 : 1000), anti-PARP ab (CST, #9532, 1 : 1000), and anti-β-actin ab (Sigma-Aldrich, A5441, 1 : 10 000). Then, the appropriate secondary mouse or rabbit antibodies coupled to horseradish peroxidase (anti-mouse: Jackson Immunoresearch Laboratories, 115035003; anti-rabbit: Jackson Immunoresearch laboratories, 111035144, 1 : 10 000) were applied and the protein bands were revealed with chemiluminescence. The band signals were quantified using the ImageJ software program.

Immunofluorescence staining

After treatment with the QD formulations at 5 μg mL^{-1} Ag concentration and the equivalent free 5FU for 48 h, the cells

were fixed in 3.7% PFA in 1× PBS, pH 7.4, for 30 min, washed with PBS and permeabilized in 1× PBS containing 0.1% saponin and 0.1% BSA. After 3 washes in 1× PBS, cover slides were incubated with the primary antibody (anti-Cleaved-Caspase-3 ab, CST, #9664, 1 : 100; anti SQSTM1/p62 ab, BD Transduct. Lab, 610832, 1 : 400; anti-LC3B ab, Sigma-Aldrich, L7543, 1 : 200) for 1 h at RT. Following 3 washes in 1× PBS, the cover slides were incubated with Alexa 568 or 488-conjugated secondary antibodies (molecular probes, 927 075, 948 490, Invitrogen, Eugene, OR) for 1 h at RT. The cells were washed 3 times and DAPI stain was added in the last wash to visualize the nuclei. The cover slides were mounted using 50% glycerol in 1× PBS and analyzed under a fluorescence microscope (Olympus BX60, Japan) using a Plan-Apochromat 60×/1.42 oil objective.

Autophagy studies

To assess the role of autophagy in EGFR-dependent 5FU induced cell death, we utilized RNAi experiments. A549 cells were transfected with shRNA against ATG5 by using linear 25 kDa polyethyleneimine (PEI; PolySciences Inc., 23 966) (1 μg mL^{-1}), which is a standard transfection agent. The downregulation of the target protein was confirmed by immunoblotting. The autophagic capacity of shATG5-A549 cells was evaluated with LC3 gel-shift assay, LC3 dot formation and P62 accumulation by immunoblotting and indirect fluorescent microscopy analysis, which we mentioned above in detail, respectively. Starvation-induced autophagy was achieved by incubating cells in EBSS (Earle's Balanced Salt Solution, Biological Industries, Cat. No.: 02-010-1A) for 4 h to study the dynamics of autophagic activity.

Statistical analysis

Statistical significance was assessed by using non-parametric Kruskall–Wallis one-way analysis of variance followed by Dunn's multiple comparisons test using the GraphPad Prism 6 software package (GraphPad Software, Inc., USA). Comparisons between only two groups were performed using the *t*-test. The data are presented as mean ± standard deviation (SD). All experiments were repeated at least three times and a value of $p < 0.05$ was considered significant. All tests were two-tailed.

Results and discussion

Preparation and characterization of Cet conjugated 5FU loaded Ag_2S QDs

In this study, 5FU was loaded onto cationic Ag_2S near-infrared emitting QDs tagged with cetuximab for selective delivery of the drug/nanoparticle complex to EGFR positive cancer cells *via* receptor-mediated endocytosis. These nanoparticles were prepared as described in Scheme 1. First, Ag_2S QDs were synthesized from the Ag and S precursors in a very simple one step aqueous synthetic route with a mixed coating comprised of branched PEI (25 kDa MW) and 2MPA at RT.[56] PEI provides colloidal stability but does not form luminescent particles. Yet, use of 2MPA as a co-stabilizer reduces the defects on the crystal surface and produces particles with strong luminescence intensity, eliminating non-radiative events.[56] As we showed previously, these PEI/2MPA coated cationic Ag_2S QDs luminesce in the NIR spectral region with a peak maximum around 800 nm and a quantum yield *ca.* 50% higher than LDS 798 NIR dye (14% QY in MeOH) as well as small hydrodynamic sizes under 50 nm (Fig. 1a and Table 1). Their functional surface is very useful for drug loading, while the small hydrodynamic size is highly critical in escaping reticulo-endothelial system (RES) uptake.[59] However, the use of cationic nanoparticles is still limited due to their *in vivo* cytotoxicity but is still advantageous for high cellular internalization.[60] The most common way to enhance the biocompatibility of nanoparticles is to conjugate PEG to the nanoparticle surfaces. PEG functionalization of the surfaces enhances the dispersion and circulation time of the nanoparticles in the blood and reduces nonspecific protein

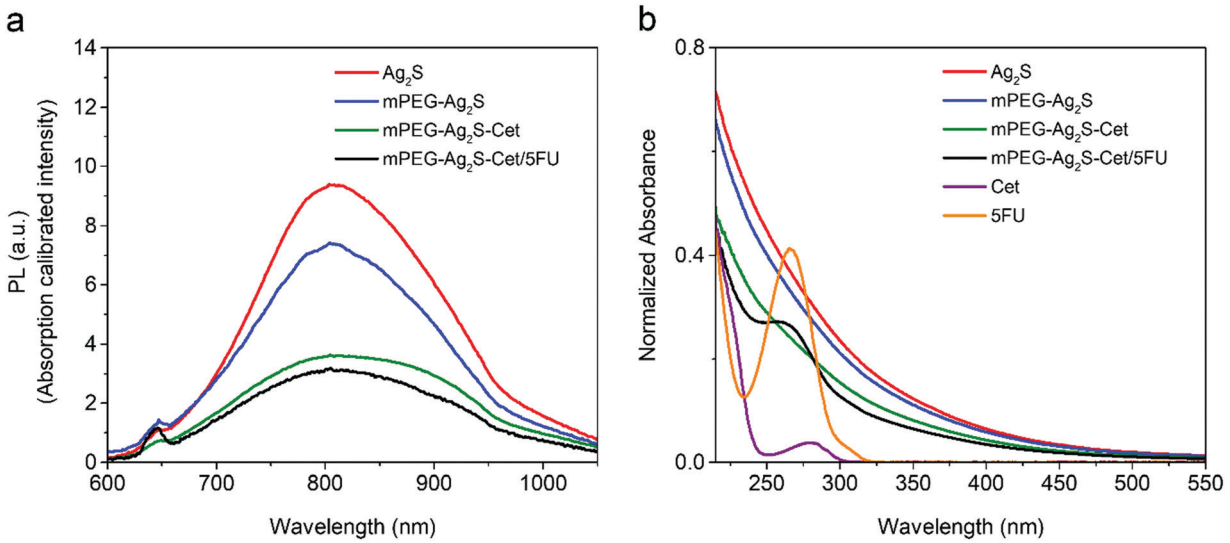

Fig. 1 Photoluminescence (a) and corresponding absorbance spectra (b) of QDs and absorbance spectra of free Cet and free 5FU.

binding as well as macrophage engulfment, and thereby rapid renal clearance through RES capture of the particles by organs such as the liver and kidneys. In this way, PEGylation facilitates the accumulation of the compositions at the tumour sites with an enhanced permeability and retention effect (EPR).[61,62] Therefore, in order to decrease the cytotoxicity of the cationic PEI surface and increase the drug loading capacity and blood circulation time of the nanoparticles, we have PEGylated Ag_2S QDs using mPEG–OH (2 kDa MW) after activation by CDI (Scheme 1). Then, the mPEG–Ag_2S QDs were conjugated with Cet to target EGFR overexpressing cancer cells. To increase the availability of the Cet ligand to the EGF receptors, a PEG linker (amine–PEG–VA, 3.4 kDa) with a larger molecular weight than mPEG–OH was used between the QD and Cet antibody. Briefly, amine–PEG–VA was first conjugated to mPEG–Ag_2S QDs and then Cet was bound to this linker *via* EDC/NHS chemistry. The conjugation efficiency of Cet to the QDs was calculated to be 52.2% by Bradford assay. This corresponds to 0.00765 mg (0.05 nmol) Cet per mg of mPEG–Ag_2S–Cet QDs (0.765% w/w). Cet has a characteristic absorption peak at 280 nm as shown in Fig. 1b. However, after conjugation of Cet to the QDs, this peak was dominated by the strong absorption peak of the QDs at these wavelengths.

Finally, the mPEG–Ag_2S–Cet QDs were loaded with 5FU, which may be considered as an anionic anticancer drug. The cationic PEI coating and PEGylated surface of the Ag_2S QDs contribute to the electrostatic and hydrophobic interaction between the drug and QDs and enhance the drug loading efficiency. Absorbance spectra of the samples clearly demonstrate that the mPEG–Ag_2S–Cet QDs were efficiently loaded with 5FU. The hump in the absorbance curve of the mPEG–Ag_2S–Cet/5FU QDs fits very well with the characteristic absorbance peak of free 5FU at 265 nm as shown in Fig. 1b. The 5FU encapsulation efficiency (EE%) of the QDs was calculated to be 57.8% from a calibration curve prepared by concentration-dependent absorption of 5FU at 265 nm. The drug loading efficiency (LE%) was calculated to be 7.34%. This equals 0.0734 mg (0.56 μmol) 5FU per mg of mPEG–Ag_2S–Cet/5FU QDs (7.34% w/w).

The Ag_2S QDs with the PEI/2MPA coating showed a strong emission maximum at 807 nm which decreases slightly after PEGylation (Fig. 1a). Cet conjugation caused a more dramatic decrease in the emission intensity without a significant shift in the peak position. 5FU loading also caused a minor drop in the emission intensity and the overall particles, mPEG–Ag_2S–Cet/5FU QDs, had about 1/3 of the original intensity of the Ag_2S QDs. However, the QDs still have strong emission intensities for diagnostic applications when we consider the strong *in vivo* emission intensities of the Ag_2S QDs with a 15.5% QY (with respect to the NIR standard dye IR-26, 0.5% QY in 1,2-dichloroethane) or with a 2.1% QY (with respect to the indocyanine green reference standard, 13% QY in DMSO) reported previously.[30,63,64]

DLS and zeta potential measurements in PBS solution proved that all QDs are in small hydrodynamic sizes and surface functionalization did not cause any dramatic aggregation (Table 1). The average number based hydrodynamic size of the Ag_2S QDs was 7.4 ± 0.6 nm with a zeta potential of 11.8 ± 1.2 mV. When the nanoparticles were PEGylated (mPEG–Ag_2S QDs), the hydrodynamic size increased to 15.2 ± 1.0 nm, whereas the zeta potential decreased to 2.4 ± 1.0 mV. This was expected, since PEG should increase the hydrated shell thickness and should reduce the overall net cationic charge due to its anionic contribution. Cet conjugation and 5FU loading did not change the size significantly compared to the PEGylated QDs. So, all these particles are still under 50 nm and can be considered as ultrasmall, which is critical for effective receptor-mediated targeting and long blood circulation times.

Optical imaging and molecular targeting

To evaluate the potential of the synthesized QDs as optical imaging agents and confirm the impact of functionalization with PEG and Cet on cell uptake, fluorescence microscopy was used. A549 and H1299 cells were incubated with Ag_2S, mPEG–Ag_2S, mPEG–Ag_2S–Cet and mPEG–Ag_2S–Cet/5FU QDs at 5 μg Ag per mL concentration for 24 h. Internalization of QDs and generation of intracellular optical signal were confirmed with an inverted fluorescence microscope equipped with a NIR filter set. In the images shown in Fig. 2, the red color indicates the NIR signal originating from the QDs and the blue color represents the cell nuclei stained with DAPI. Overall, all the images demonstrate strong intracellular emission originating from QDs distributed mostly in the cytoplasm of the cells. A549 adenocarcinomic human alveolar basal epithelial cells are strong EGFR expressors while H1299 human non-small cell lung carcinoma cells are poor expressors of EGFR. The strong NIR signal from the cells treated with Ag_2S QDs indicates high uptake of these cationic nanoparticles in a non-selective manner by both cell lines. Control cells without QD treatment underlined that the NIR signal of the QDs is significantly stronger than the weak autofluorescence of the cells seen at these wavelengths.

Table 1 Characterization of QDs

Sample name	Size[b] (nm)	PDI[c]	ζ potential[d] (mV)	Ag content[e] (weight%)	Cet content[f] (weight%)	5FU content[g] (weight%)
Ag_2S[a]	7.4 ± 0.6	0.348 ± 0.047	11.8 ± 1.2	11.45	—	
mPEG–Ag_2S	15.2 ± 1.0	0.357 ± 0.015	2.4 ± 1.0	4.60	—	
mPEG–Ag_2S–Cet	14.3 ± 0.9	0.332 ± 0.008	0.3 ± 0.2	4.21	0.765	—
mPEG–Ag_2S–Cet/5FU	14.8 ± 2.0	0.406 ± 0.062	1.6 ± 0.3	4.81	0.874	7.34

[a] Ag_2S is coated with PEI/2MPA. [b] Hydrodynamic size measured by dynamic light scattering and reported as a number-based average. [c] Polydispersity index of the hydrodynamic size. [d] Surface charge. [e] Measured by ICP-MS. [f] Calculated by Bradford Assay. [g] Calculated from the absorbance at 265 nm using a 5FU calibration curve.

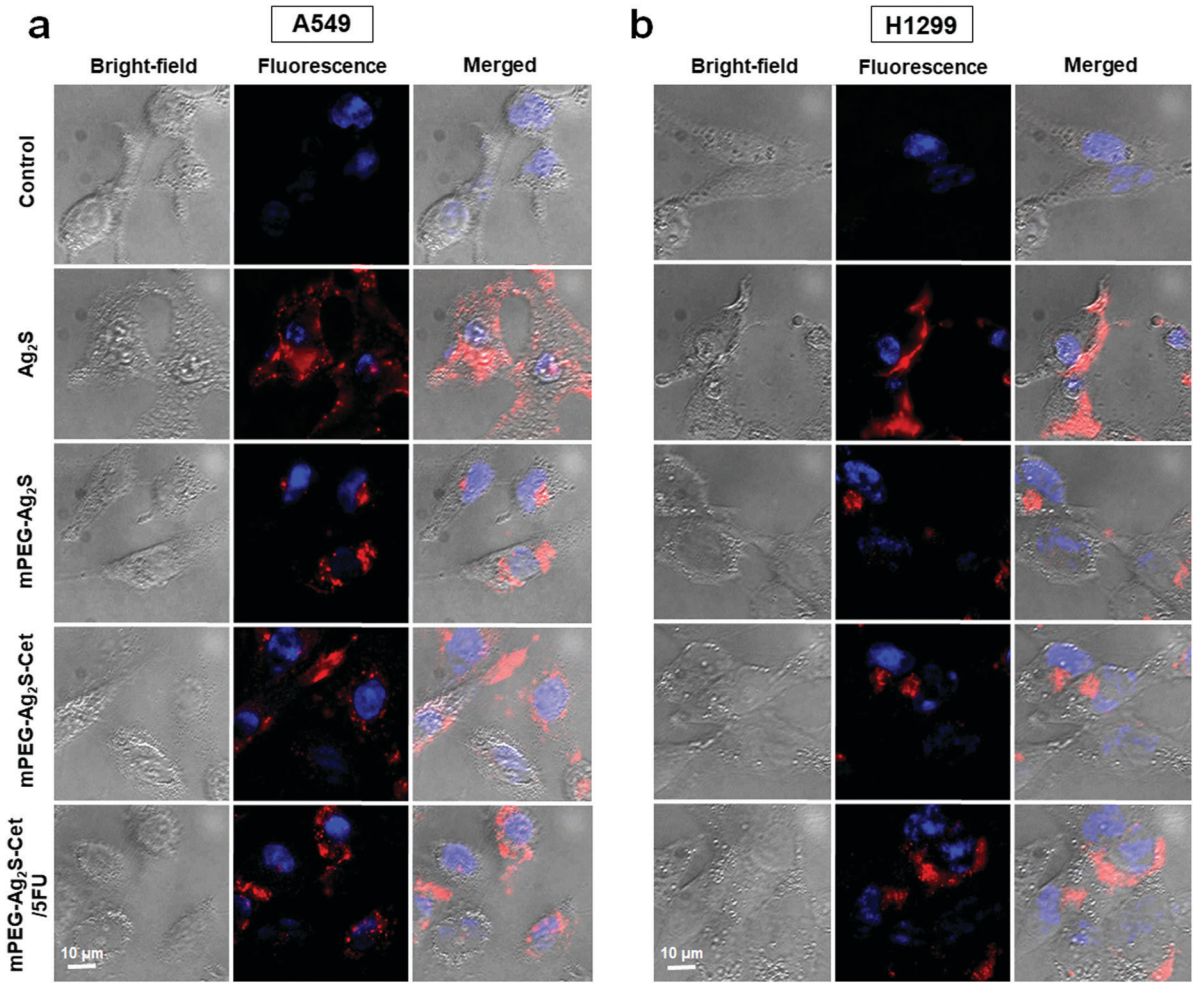

Fig. 2 Fluorescence microscopy images of A549 (a) and H1299 (b) cells incubated with Ag_2S, mPEG–Ag_2S, mPEG–Ag_2S–Cet and mPEG–Ag_2S–Cet/5FU at 5 μg mL^{-1} Ag concentration for 24 h. Untreated cells were used as controls. Bright-field and corresponding fluorescence images (NIR and DAPI) were presented with their merged images for all compositions in both cell lines. Red signals indicate QD emission at NIR wavelengths; blue signals indicate DAPI staining in cell nuclei. The scale bar shows 10 μm.

The internalization of Ag_2S QDs in A549 cells seems similar to H1299 cells but they are better dispersed in the cytoplasm of A549 than H1299. The reduced NIR signal with PEGylated Ag_2S QDs indicates the reduced internalization of the nanoparticles. This trend is quite meaningful, since cationic nanoparticles are internalized by the cells quite easily due to electrostatic interaction with the negatively charged cell surface. PEGylation both reduces this strong cationic charge and masks the nanoparticle surface creating a hydrophilic barrier that sterically prevents protein adsorption. This increases the biocompatibility of the structures partially due to a decrease of the cell internalization and cationic charge, which mostly causes mitochondrial and lysosomal damage as well as disruption of the plasma-membrane integrity.[60,65–67]

Cet conjugation to PEGylated nanoparticles resulted in efficient cellular uptake and endosomal localization of QDs in both cell lines but more in A549 cells, as desired. The stronger NIR signal clearly indicates higher uptake of Cet conjugated QDs by strong EGFR overexpressing A549 cells than H1299, implying effective receptor-mediated endocytosis (Fig. 2). Further studies performed with 5FU-loaded mPEG–Ag_2S–Cet QDs also indicated a similar trend presenting higher NIR signal in the A549 cells. These results clearly show that Ag_2S QDs are promising optical imaging tools for targeted drug delivery applications in cancer diagnosis and therapy, and they can be selectively and effectively delivered to EGFR overexpressing tumour cells when conjugated with Cet.

Assessment of *in vitro* cytotoxicity

The dose dependent cytotoxicity of these QDs was evaluated in A549 and H1299 cells. The dosing was based on their Ag content measured by ICP-MS to keep the number of particles constant for each formulation. The viability of cells that were incubated with QDs in a concentration range between 0.1 and 7.5 μg Ag per mL for 48 h was measured by MTT assay. Free Cet (0.0182–1.365 μg mL^{-1}) and free 5FU (0.153–11.5 μg mL^{-1}) at equivalent concentrations to their amount in the QDs were used as controls. The viability of both A549 and H1299 cells that were treated with cationic Ag_2S QDs dropped significantly with increasing concentrations of the QDs (Fig. 3). The IC_{50}

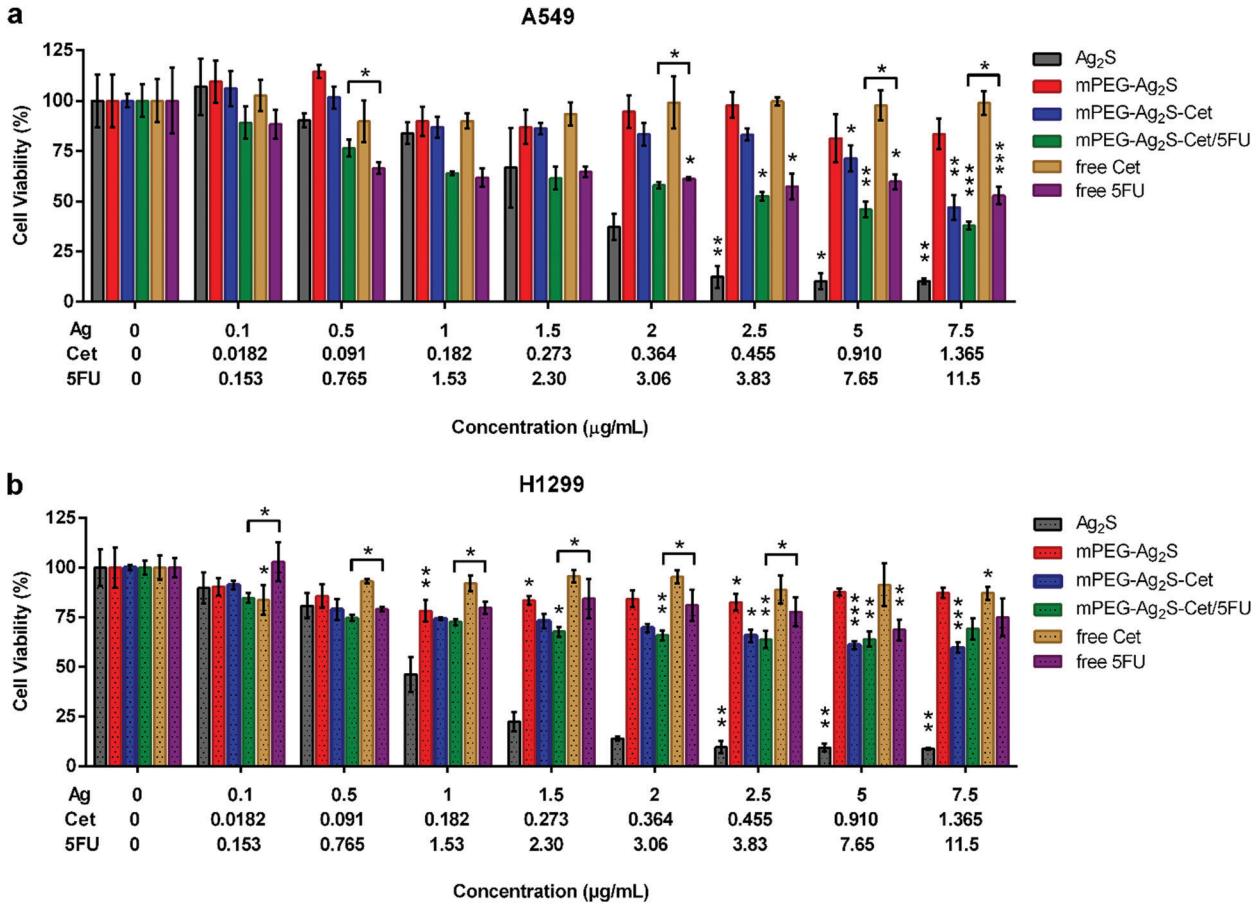

Fig. 3 Cell viability of A549 (a) and H1299 (b) cells treated with the samples for 48 h, performed by MTT assay. Untreated cells were accepted as a control. The data were expressed as mean ± S.D. (n = 4), $p < 0.05$ (*), $p < 0.01$ (**) and $p < 0.001$ (***). The stars show the statistical significance of each data point from the control. The stars with arrows indicate a significant difference between free 5FU and 5FU/mPEG–Ag_2S–Cet QDs.

(half maximal inhibitory concentration) value for the A549 cells was determined as 1.78 μg Ag per mL (Fig. 3a). The H1299 cells showed a more vulnerable nature against Ag_2S QDs with an IC_{50} value of 0.95 μg Ag per mL (Fig. 3b). After PEGylation of Ag_2S QDs, the cell viability dramatically increased above 80%. Indeed, PEGylation was shown to decrease the cellular uptake of nanoparticles, and enhance their biocompatibility as mentioned previously.[62,68] Once the toxicity of the particle is reduced, now it is important to direct them to the cancer cells. Cet conjugation to PEGylated QDs enhanced their internalization by EGFR overexpressing cells (Fig. 2a). This was achieved with mPEG–Ag_2S–Cet nanoparticles, which significantly decreased the viability in both cell lines (Fig. 3a and b). The IC_{50} value of the QDs for A549 cells was increased to 7.18 μg Ag per mL while the cell viability in H1299 remained over 50% even at high concentrations of mPEG–Ag_2S–Cet QDs, despite the more vulnerable nature of H1299 against cationic QDs. This suggests a much higher cellular uptake of the nanoparticles in A549 than H1299 cells due to stronger EGFR expression of the former. Another important point is that free Cet showed almost no toxicity at these doses. The cell viability was around 100% in A549 cells and about 87% in H1299 cells at a concentration of 1.365 μg mL^{-1} Cet, which is equivalent to the amount present in the highest dose (7.5 μg Ag per mL) of mPEG–Ag_2S–Cet QDs. This implies that conjugation of the antibody onto the QDs improved the cellular accumulation of the nanoparticles by receptor-mediated uptake but did not contribute to the toxicity. Chemotherapeutic drug 5FU barely hit IC_{50} and only for A549 at the highest dose (11.5 μg mL^{-1}) when administered as a free drug. The viability of H1299 cells stayed around 75%. This indicates that the 5FU dose range studied here is low for effective treatment if 5FU were used as a free drug. On the other hand, 5FU loaded mPEG–Ag_2S–Cet QDs reduced the viability of A549 cells effectively (Fig. 3a) with an IC_{50} of 3.49 μg Ag per mL, which corresponds to 5.34 μg 5FU per mL. However, no significant enhancement of the cytotoxic effect was recorded for 5FU-loaded mPEG–Ag_2S–Cet QDs on H1299 cells (Fig. 3b). This was expected since Cet would not dramatically enhance the uptake of 5FU loaded QDs into low EGFR-expressing H1299 cells. There seems to be lower viability at 2.3–3.8 μg 5FU per mL doses when 5FU/mPEG–Ag_2S–Cet QDs were used, but the about 63–73% viability at these doses is identical to the results obtained with only mPEG–Ag_2S–Cet QDs. Hence, it is not possible to attribute the drop in viability to targeted delivery of 5FU to H1299. Overall, these results confirm the significance of selective targeting of 5FU to EGFR overexpressing cancer

cells *via* antibody conjugated QDs for an enhanced therapeutic effect.

Effect of QDs on cell death

The cell death of both cell lines treated with all four QDs (5 μg per mL Ag), equivalent free 5FU (7.65 μg mL^{-1}) and equivalent free Cet (0.91 μg mL^{-1}) was investigated *via* FACS analysis (Fig. 4). 5FU alone showed about 20% cell death, more in A549 cells (Fig. 4c). In addition, the free drug induced both apoptotic and necrotic cell death in both lung cancer cell lines, yet the amount of necrotic cell death was more prominent in comparison to apoptotic cell death especially in strong EGFR overexpressing A549 cells (Fig. 4d and e). Cet alone did not exert any significant cell death in either cell line. Cationic Ag_2S QDs caused aberrant necrotic cell death with no cell specificity (Fig. 4e). However, PEGylation reduced the cell death significantly in both cell lines in agreement with the MTT assay results, by forming a highly biocompatible surface on the nanoparticles. Cet conjugation to these PEGylated structures created a great difference in the response of these two cell lines. About 40% death in A549 cells compared to non-significant death in H1299 cells treated with mPEG–Ag_2S–Cet/5FU along with enhanced apoptotic death was determined. Strikingly, mPEG–Ag_2S–Cet/5FU formulation exclusively increased apoptotic cell death in lung cancer cells in an EGFR status dependent manner.

Further analysis utilizing established molecular markers of apoptotic cell death activation, caspase-3 activation and PARP cleavage, was performed in both cell lines.[69] As shown in Fig. 5a, we observed that 5FU increased cleaved-caspase-3 staining in EGFR overexpressing A549 cells. But, mPEG–Ag_2S–Cet/5FU treatment caused more prominent cleaved-caspase-3 staining in comparison to free 5FU treatment. In line with this, PARP cleavage and caspase-3 activation were observed only in high EGFR overexpressing cells upon treatment with mPEG–Ag_2S–Cet/5FU and its effect was more pronounced than free

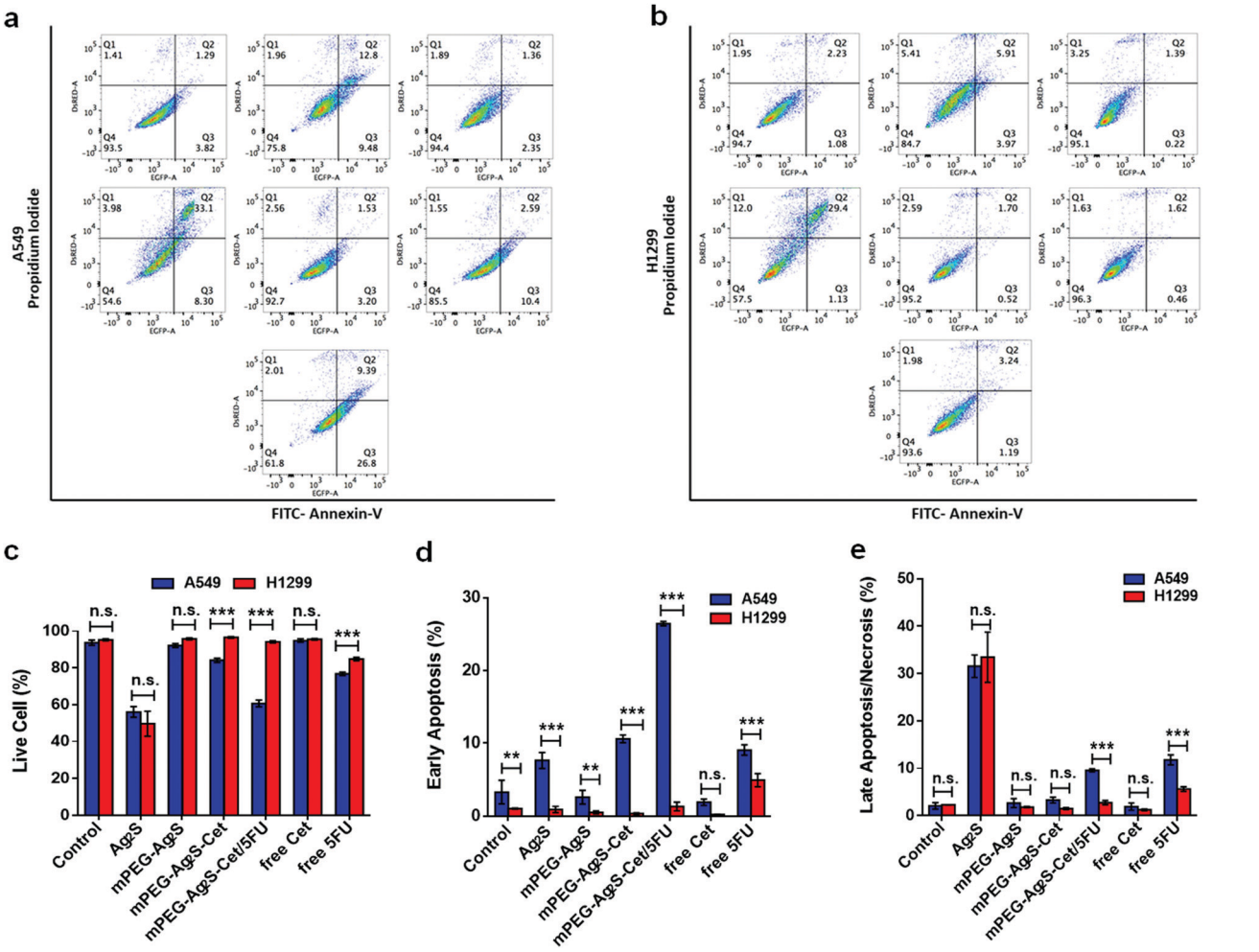

Fig. 4 Cytotoxicity and cell death analysis of QDs by FACS measurements using Annexin V/PI staining on A549 (a) and H1299 lung cancer cells (b). Cells were treated with various QD formulations at 5 μg per mL Ag concentration and equivalent free Cet (0.91 μg mL^{-1}) and free 5FU (7.65 μg mL^{-1}) for 48 h. FACS results show live cells (c), defined as Annexin V-negative and PI-negative cells; early apoptosis (d), defined as Annexin V-positive and PI-negative cells; and late apoptosis (e), defined as Annexin V-positive and PI-positive cells. Data were presented as mean ± SD of independent experiments (n = 3). $p < 0.05$ (*), $p < 0.01$ (**) and $p < 0.001$ (***). n.s.: not significant.

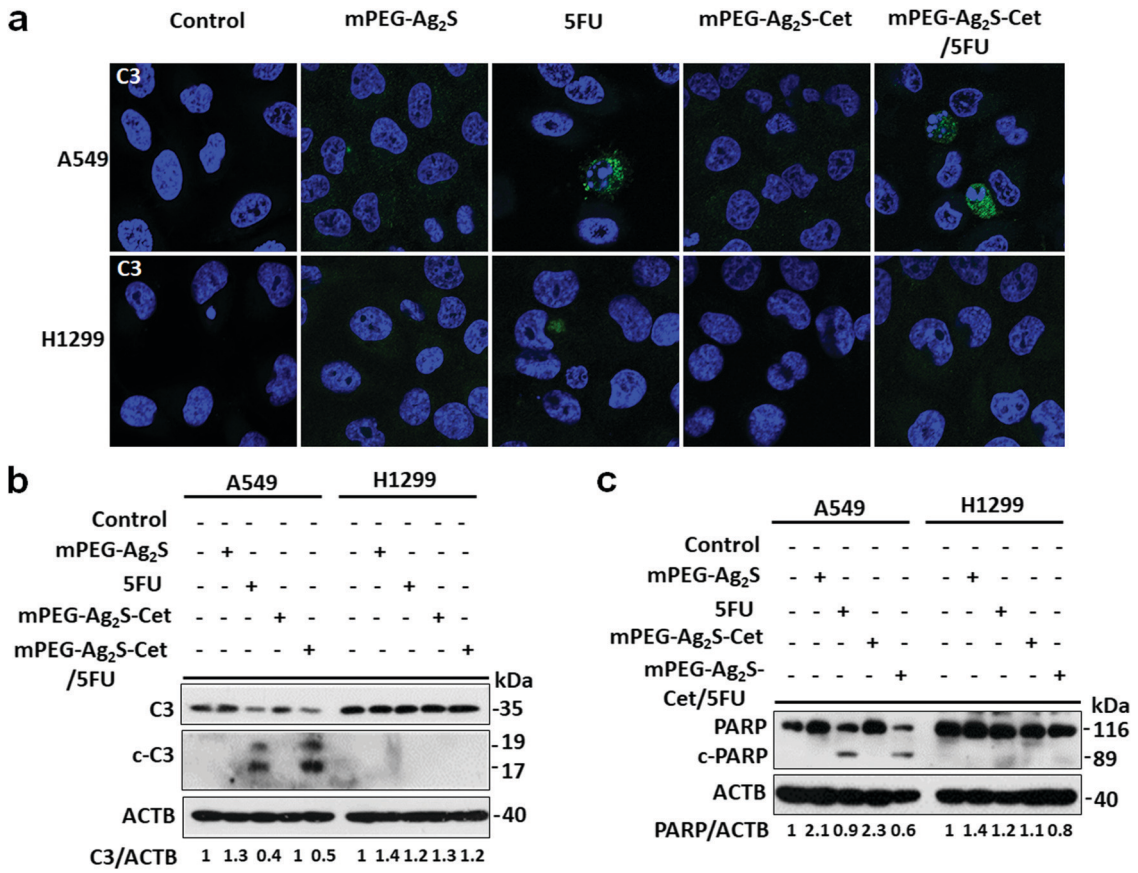

Fig. 5 EGFR targeted QDs mitigate apoptosis induced by 5FU in lung cancer. Cells were treated with various formulations of QDs at 5 μg per mL Ag concentration and equivalent free 5FU (7.65 μg mL^{-1}) for 48 h. Caspase-3 (C3, Alexa-488-green) activation (a). Hallmarks of apoptosis were analyzed by immunofluorescence staining followed by confocal microscopy under 63× magnification using a Carl Zeiss LSM 710 confocal microscope. Cleavage of Caspase-3 (b) and PARP (c) was evaluated by immunoblotting.

5FU treatment (Fig. 5b and c). Conversely, EGFR low cells exposed to mPEG–Ag_2S–Cet/5FU had no activation of apoptosis markers under the given experimental conditions (Fig. 5).

Effects of QDs on drug-induced autophagy

Drug resistance has been reported as one of the most important obstacles in front of effective treatment of cancer.[70] According to previous studies, autophagy attenuates the efficacy of the treatment by protecting cells from death.[48,54,71] As shown in Fig. 6a and b, we found that treatment with free 5FU increases autophagy in both cell lines. Interestingly, we also observed that 5FU-induced autophagy was abolished in mPEG–Ag_2S–Cet/5FU treatment specifically in targeted A549 cells, which supports that drug-induced autophagy might require EGFR signal transduction. In order to confirm the exact role of autophagy in our system, we created autophagy deficient A549 cells upon knocking down ATG5 by RNAi. ATG5 is a core protein and responsible for the elongation of the autophagosome. The absence of ATG5 blocks the LC3 shift and LC3 puncta formation (Fig. 6b and c) and further causes the accumulation of p62, an autophagic receptor protein, which is normally degraded upon autophagic stimuli (Fig. 6c). Strikingly, 5FU exerts a more prominent anti-cancer effect on autophagy deficient cells in comparison to the wild type counterparts. Here, we discovered that 5FU-induced autophagy dependent drug resistance may be hindered by our designed QDs, mPEG–Ag_2S–Cet/5FU. Therefore, our QD formulation, mPEG–Ag_2S–Cet/5FU, emerges as a good candidate for a multi-modal therapeutic approach to treat EGFR+ lung cancer.

Conclusions

NIR emitting Ag_2S QDs with a PEI/2MPA coating conjugated with Cet were demonstrated in this study as highly specific and effective 5FU delivering theranostic nanoparticles to EGFR-overexpressing lung cancer cells. While cationic nanoparticles are quite toxic, PEGylation both reduced the toxicity and non-specific uptake and enhanced the loading of 5FU onto the polymeric corona. These quite small QDs consist of 7.34 wt% 5FU and 0.874 wt% Cet, which could not provide sufficient treatment efficacy when used as free drugs. *In vitro* toxicity studies were conducted with EGFR low expressor H1299 and high expressor A549 cell lines in a dose dependent manner. Cet conjugation to PEGylated QDs decreased their biocompatibility particularly in A549 cells due to higher intracellular accumulation and resulted

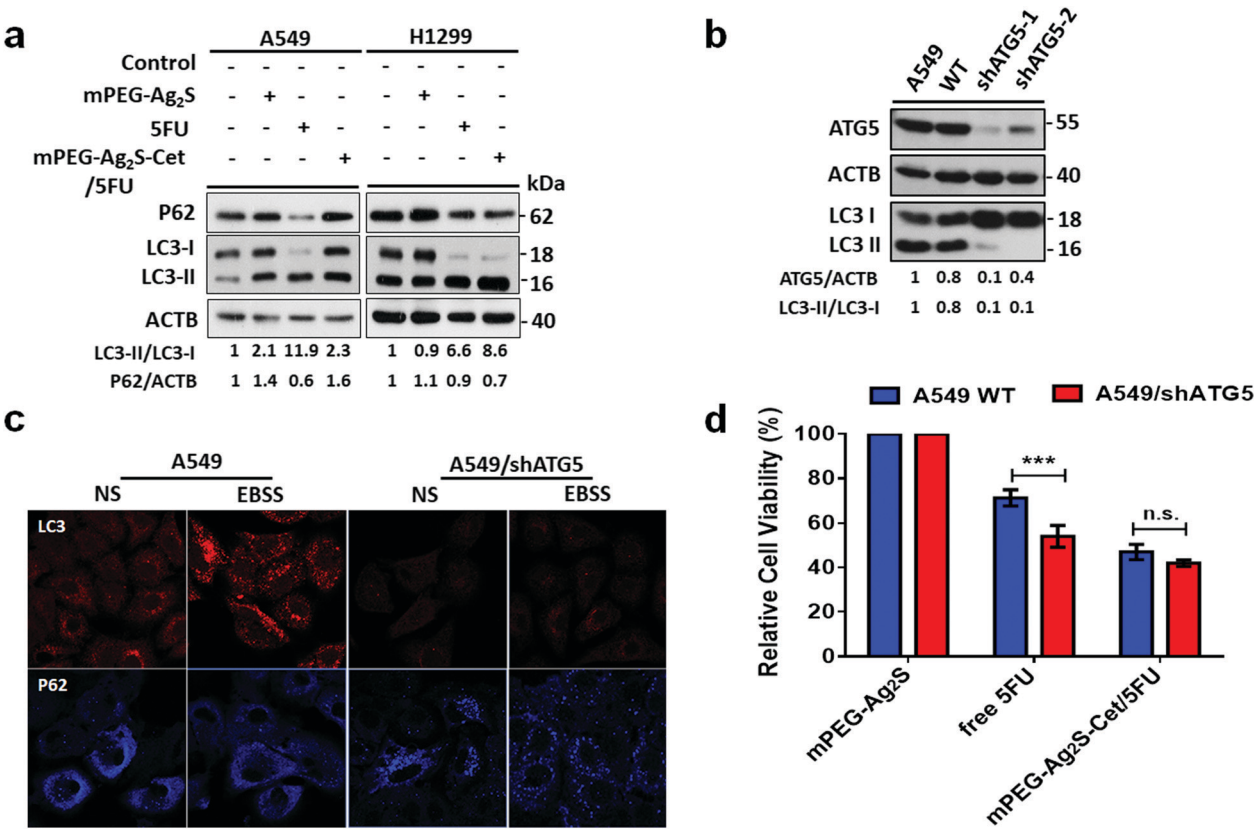

Fig. 6 Autophagy analysis. EGFR targeted QDs block cytoprotective autophagy to overcome 5FU resistance in lung cancer. Cells were treated with various formulations of QDs at 5 μg per mL Ag concentration and equivalent free 5FU (7.65 μg mL^{-1}) for 48 h. P62 receptor degradation and LC3 shift evaluated by immunoblotting (a). Autophagy attenuated A549 cells were created and characterized by immunoblotting (b). Immunofluorescent analysis of the ATG5 level and LC3 shift of autophagy attenuated cells (c). NS: non-starved; EBSS: starved. MTT cell viability analysis was performed (d). Data were presented as mean ± SD of independent experiments (n = 3). $p < 0.05$ (*), $p < 0.01$ (**) and $p < 0.001$ (***). n.s.: not significant.

in dramatic apoptosis. The IC_{50} value of 5FU is reduced from about 11.5 μg mL^{-1} to 5.34 μg in A549 cells when delivered with mPEG–Ag_2S–Cet, but it was never reached in HT1299 cells even at the highest dose used in this study (11.5 μg 5FU per mL). This confirms that optically traceable mPEG–Ag_2S–Cet/5FU induces significant cell death, especially apoptotic cell death, more effectively than free 5FU and Cet conjugation in this amount allows selective delivery of the drug to EGFR overexpressing cells but does not contribute to toxicity.

In addition, 5FU effectively increased autophagy in both lung cancer cell lines in parallel with the literature.[48,50–53] According to the previous studies, inhibition of autophagy is suggested as a novel strategy to ameliorate the efficacy of cancer treatment. Therefore, we propose that autophagy might function as a resistance mechanism against cell death in our system. We demonstrate that the level of cell death was enhanced by inhibition of autophagy during 5FU treatment of the cells. Surprisingly, mPEG–Ag_2S–Cet/5FU alone did not show autophagic enhancement in comparison with 5FU alone. Therefore, we suggest that mPEG–Ag_2S–Cet/5FU may eliminate the necessity of adjuvant therapy since it showed suppression of 5FU-induced autophagy by itself. Thus, our multi-potent QDs provide a powerful strategy with a broad spectrum to cure EGFR+ lung cancer.

Conflicts of interest

There is no conflict of interest reported by the authors.

Acknowledgements

This work was financially sponsored by the Scientific and Technological Research Council of Turkey (grant number 113Z164). Yunus Akkoc is supported by a TUBITAK-BIDEB 2211 scholarship for PhD studies. The authors would like to thank Dr Gulsu Simsek (KUYTAM, Koc University, Istanbul, Turkey) for her assistance with ICP-MS measurements and Mahshid Hashemkhani for her help in drug loading and antibody purification studies.

References

1 R. Siegel, C. DeSantis, K. Virgo, K. Stein, A. Mariotto, T. Smith, D. Cooper, T. Gansler, C. Lerro and S. Fedewa, *Ca-Cancer J. Clin.*, 2012, **62**, 220–241.
2 R. Siegel, J. Ma, Z. Zou and A. Jemal, *Ca-Cancer J. Clin.*, 2014, **64**, 9–29.
3 S. Singhal, S. Nie and M. D. Wang, *Annu. Rev. Med.*, 2010, **61**, 359–373.

4 L. Fass, *Mol. Oncol.*, 2008, **2**, 115–152.
5 A. S. Kierans, S. K. Kang and A. B. Rosenkrantz, *Radiology*, 2015, **278**, 82–94.
6 S. Luo, E. Zhang, Y. Su, T. Cheng and C. Shi, *Biomaterials*, 2011, **32**, 7127–7138.
7 Y. T. Lim, S. Kim, A. Nakayama, N. E. Stott, M. G. Bawendi and J. V. Frangioni, *Mol. Imaging*, 2003, **2**, 50–64.
8 E. İ. Altınoğlu and J. H. Adair, *Wiley Interdiscip. Rev.: Nanomed. Nanobiotechnol.*, 2010, **2**, 461–477.
9 H. Kobayashi, M. Ogawa, R. Alford, P. L. Choyke and Y. Urano, *Chem. Rev.*, 2009, **110**, 2620–2640.
10 X. Michalet, F. Pinaud, L. Bentolila, J. Tsay, S. Doose, J. Li, G. Sundaresan, A. Wu, S. Gambhir and S. Weiss, *Science*, 2005, **307**, 538–544.
11 W. W. Yu, Y. A. Wang and X. Peng, *Chem. Mater.*, 2003, **15**, 4300–4308.
12 M. A. Hines and G. D. Scholes, *Adv. Mater.*, 2003, **15**, 1844–1849.
13 B. Blackman, D. M. Battaglia, T. D. Mishima, M. B. Johnson and X. Peng, *Chem. Mater.*, 2007, **19**, 3815–3821.
14 S. Kim, B. Fisher, H.-J. Eisler and M. Bawendi, *J. Am. Chem. Soc.*, 2003, **125**, 11466–11467.
15 S. Kim, Y. T. Lim, E. G. Soltesz, A. M. De Grand, J. Lee, A. Nakayama, J. A. Parker, T. Mihaljevic, R. G. Laurence and D. M. Dor, *Nat. Biotechnol.*, 2004, **22**, 93.
16 Y. Du, B. Xu, T. Fu, M. Cai, F. Li, Y. Zhang and Q. Wang, *J. Am. Chem. Soc.*, 2010, **132**, 1470–1471.
17 C. Li, Y. Zhang, M. Wang, Y. Zhang, G. Chen, L. Li, D. Wu and Q. Wang, *Biomaterials*, 2014, **35**, 393–400.
18 G. Chen, F. Tian, Y. Zhang, Y. Zhang, C. Li and Q. Wang, *Adv. Funct. Mater.*, 2014, **24**, 2481–2488.
19 C. Li, L. Cao, Y. Zhang, P. Yi, M. Wang, B. Tan, Z. Deng, D. Wu and Q. Wang, *Small*, 2015, **11**, 4517–4525.
20 J. Chen, L. Feng, M. Zhang, X. Zhang, H. Su and D. Cui, *Mater. Lett.*, 2013, **96**, 224–227.
21 J. Fu, L. Wang, H. Chen, L. Bo, C. Zhou and J. Chen, *Spectrochim. Acta, Part A*, 2010, **77**, 625–629.
22 Z. Han, L. Wei, L. Tang, C. Chen, H. Pan and J. Chen, *J. Power Sources*, 2013, **239**, 546–552.
23 Y. Zhang, Y. Zhang, G. Hong, W. He, K. Zhou, K. Yang, F. Li, G. Chen, Z. Liu and H. Dai, *Biomaterials*, 2013, **34**, 3639–3646.
24 E. Cassette, M. Helle, L. Bezdetnaya, F. Marchal, B. Dubertret and T. Pons, *Adv. Drug Delivery Rev.*, 2013, **65**, 719–731.
25 X. Gao, L. Yang, J. A. Petros, F. F. Marshall, J. W. Simons and S. Nie, *Curr. Opin. Biotechnol*, 2005, **16**, 63–72.
26 A. M. Smith, H. Duan, A. M. Mohs and S. Nie, *Adv. Drug Delivery Rev.*, 2008, **60**, 1226–1240.
27 G. Chen, F. Tian, Y. Zhang, Y. Zhang, C. Li and Q. Wang, *Adv. Funct. Mater.*, 2014, **24**, 2481–2488.
28 Y. Wang and X.-P. Yan, *Chem. Commun.*, 2013, **49**, 3324–3326.
29 J. Schroeder, I. Shweky, H. Shmeeda, U. Banin and A. Gabizon, *J. Controlled Release*, 2007, **124**, 28–34.
30 Y. Zhang, G. Hong, Y. Zhang, G. Chen, F. Li, H. Dai and Q. Wang, *ACS Nano*, 2012, **6**, 3695–3702.
31 H. Chen, B. Li, M. Zhang, K. Sun, Y. Wang, K. Peng, M. Ao, Y. Guo and Y. Gu, *Nanoscale*, 2014, **6**, 12580–12590.
32 F. D. Duman, M. Erkisa, R. Khodadust, F. Ari, E. Ulukaya and H. Y. Acar, *Nanomedicine*, 2017, **12**, 2319–2333.
33 D. Asik, M. Yagci, F. D. Duman and H. Y. Acar, *J. Mater. Chem. B*, 2016, **4**, 1941–1950.
34 L. Zhu, J. Ma, N. Jia, Y. Zhao and H. Shen, *Colloids Surf., B*, 2009, **68**, 1–6.
35 R. Singh and J. W. Lillard Jr, *Exp. Mol. Pathol.*, 2009, **86**, 215–223.
36 L. Zhang, F. Gu, J. Chan, A. Wang, R. Langer and O. Farokhzad, *Clin. Pharmacol. Ther.*, 2008, **83**, 761–769.
37 P. Wee and Z. Wang, *Cancers*, 2017, **9**, 52.
38 E. S. Kim, *Clin. Lung Cancer*, 2004, **6**, S80–S84.
39 H.-W. Kao, Y.-Y. Lin, C.-C. Chen, K.-H. Chi, D.-C. Tien, C.-C. Hsia, W.-J. Lin, F.-D. Chen, M.-H. Lin and H.-E. Wang, *Nanotechnology*, 2014, **25**, 295102.
40 M. Creixell, A. C. Bohorquez, M. Torres-Lugo and C. Rinaldi, *ACS Nano*, 2011, **5**, 7124–7129.
41 L. Milane, Z.-f. Duan and M. Amiji, *Nanomedicine*, 2011, **7**, 435–444.
42 L. Milane, Z. Duan and M. Amiji, *PLoS One*, 2011, **6**, e24075.
43 Y. Qian, M. Qiu, Q. Wu, Y. Tian, Y. Zhang, N. Gu, S. Li, L. Xu and R. Yin, *Sci. Rep.*, 2014, **4**, 7490.
44 K. Kelly, R. Herbst, J. Crowley, J. McCoy, J. Atkins, P. Lara Jr, S. Dakhil, K. Albain, E. Kim and D. Gandara, *J. Clin. Oncol.*, 2006, **24**, 7015.
45 J. B. Vermorken, R. Mesia, F. Rivera, E. Remenar, A. Kawecki, S. Rottey, J. Erfan, D. Zabolotnyy, H.-R. Kienzer and D. Cupissol, *N. Engl. J. Med.*, 2008, **359**, 1116–1127.
46 M. Petaccia, M. Condello, L. Giansanti, A. La Bella, F. Leonelli, S. Meschini, D. G. Villalva, E. Pellegrini, F. Ceccacci and L. Galantini, *MedChemComm*, 2015, **6**, 1639–1642.
47 J. L. Arias, *Molecules*, 2008, **13**, 2340–2369.
48 J. Li, N. Hou, A. Faried, S. Tsutsumi and H. Kuwano, *Eur. J. Cancer*, 2010, **46**, 1900–1909.
49 H.-y. Xiong, X.-l. Guo, X.-x. Bu, S.-s. Zhang, N.-n. Ma, J.-r. Song, F. Hu, S.-f. Tao, K. Sun and R. Li, *Cancer Lett.*, 2010, **288**, 68–74.
50 T. R. O'Donovan, G. C. O'Sullivan and S. L. McKenna, *Autophagy*, 2011, **7**, 509–524.
51 M. De la Cruz-Morcillo, M. Valero, J. Callejas-Valera, L. Arias-Gonzalez, P. Melgar-Rojas, E. Galan-Moya, E. García-Gil, J. García-Cano and R. Sánchez-Prieto, *Oncogene*, 2012, **31**, 1073.
52 J.-C. Tang, Y.-L. Feng, X. Liang and X.-J. Cai, *Chin. Med. J.*, 2016, **129**, 456.
53 X. Sui, N. Kong, X. Wang, Y. Fang, X. Hu, Y. Xu, W. Chen, K. Wang, D. Li and W. Jin, *Sci. Rep.*, 2014, **4**, 4694.
54 X. Pan, X. Zhang, H. Sun, J. Zhang, M. Yan and H. Zhang, *PLoS One*, 2013, **8**, e56679.
55 X. Liang, J. Tang, Y. Liang, R. Jin and X. Cai, *Cell Bioscience*, 2014, **4**, 10.
56 F. D. Duman, I. Hocaoglu, D. G. Ozturk, D. Gozuacik, A. Kiraz and H. Y. Acar, *Nanoscale*, 2015, **7**, 11352–11362.
57 G. Chen, W. Chen, Z. Wu, R. Yuan, H. Li, J. Gao and X. Shuai, *Biomaterials*, 2009, **30**, 1962–1970.
58 P. J. M. Michael, D. Abramoff and S. J. Ram, *Biophoton. Int.*, 2004, **11**, 36–42.

59 C. He, Y. Hu, L. Yin, C. Tang and C. Yin, *Biomaterials*, 2010, **31**, 3657–3666.
60 E. Fröhlich, *Int. J. Nanomed.*, 2012, **7**, 5577.
61 Q. He, J. Zhang, J. Shi, Z. Zhu, L. Zhang, W. Bu, L. Guo and Y. Chen, *Biomaterials*, 2010, **31**, 1085–1092.
62 H. Meng, M. Xue, T. Xia, Z. Ji, D. Y. Tarn, J. I. Zink and A. E. Nel, *ACS Nano*, 2011, **5**, 4131–4144.
63 G. Hong, J. T. Robinson, Y. Zhang, S. Diao, A. L. Antaris, Q. Wang and H. Dai, *Angew. Chem., Int. Ed.*, 2012, **51**, 9818–9821.
64 P. Jiang, C.-N. Zhu, Z.-L. Zhang, Z.-Q. Tian and D.-W. Pang, *Biomaterials*, 2012, **33**, 5130–5135.
65 J. J. Verhoef and T. J. Anchordoquy, *Drug Delivery Transl. Res.*, 2013, **3**, 499–503.
66 S. Bhattacharjee, L. H. de Haan, N. M. Evers, X. Jiang, A. T. Marcelis, H. Zuilhof, I. M. Rietjens and G. M. Alink, *Part. Fibre Toxicol.*, 2010, **7**, 25.
67 M. G. Bexiga, J. A. Varela, F. Wang, F. Fenaroli, A. Salvati, I. Lynch, J. C. Simpson and K. A. Dawson, *Nanotoxicology*, 2011, **5**, 557–567.
68 Q. He, Z. Zhang, F. Gao, Y. Li and J. Shi, *Small*, 2011, **7**, 271–280.
69 S. Elmore, *Toxicol. Pathol.*, 2007, **35**, 495–516.
70 G. Housman, S. Byler, S. Heerboth, K. Lapinska, M. Longacre, N. Snyder and S. Sarkar, *Cancers*, 2014, **6**, 1769–1792.
71 Y. Akkoç, Ö. Berrak, E. D. Arısan, P. Obakan, A. Çoker-Gürkan and N. Palavan-Ünsal, *Biomed. Pharmacother.*, 2015, **71**, 161–171.